Amplitude-Dependent Spike-Broadening and Enhanced Ca^{2+} Signaling in GnRH-Secreting Neurons

Fredrick Van Goor,* Andrew P. LeBeau,† Lazar Z. Krsmanovic,* Arthur Sherman,† Kevin J. Catt,* and Stanko S. Stojilkovic*

*Endocrinology and Reproduction Research Branch, National Institute of Child Health and Human Development, and †Mathematical Research Branch, National Institute of Diabetes and Digestive and Kidney Disease, National Institutes of Health, Bethesda, Maryland 20892 USA

ABSTRACT In GnRH-secreting (GT1) neurons, activation of Ca^{2+}-mobilizing receptors induces a sustained membrane depolarization that shifts the profile of the action potential (AP) waveform from sharp, high-amplitude to broad, low-amplitude spikes. Here we characterize this shift in the firing pattern and its impact on Ca^{2+} influx experimentally by using prerecorded sharp and broad APs as the voltage-clamp command pulse. As a quantitative test of the experimental data, a mathematical model based on the membrane and ionic current properties of GT1 neurons was also used. Both experimental and modeling results indicated that inactivation of the tetrodotoxin-sensitive Na^+ channels by sustained depolarization accounted for a reduction in the amplitude of the spike upstroke. The ensuing decrease in tetraethylammonium-sensitive K^+ current activation slowed membrane repolarization, leading to AP broadening. This change in firing pattern increased the total L-type Ca^{2+} current and facilitated AP-driven Ca^{2+} entry. The leftward shift in the current-voltage relation of the L-type Ca^{2+} channels expressed in GT1 cells allowed the depolarization-induced AP broadening to facilitate Ca^{2+} entry despite a decrease in spike amplitude. Thus the gating properties of the L-type Ca^{2+} channels expressed in GT1 neurons are suitable for promoting AP-driven Ca^{2+} influx in receptor- and non-receptor-depolarized cells.

INTRODUCTION

In cells expressing voltage-gated Ca^{2+} channels (VGCCs), action potential (AP) firing promotes Ca^{2+} entry, which triggers a variety of biochemical events involved in the control of cell function. The frequency, amplitude, duration, and rate of rise and fall of AP-driven Ca^{2+} signals determine the magnitude and/or specificity of the cellular response (Spencer et al., 1989; Hsu et al., 1996; Dolmetsch et al., 1997; De Konninck and Schulman, 1998; Charles et al., 1999). In general, the profile of the AP waveform and the gating properties of the VGCCs determine the peak and duration of the voltage-gated Ca^{2+} current (I_{Ca}), which in turn dictate the pattern of Ca^{2+} influx. Consequently, changes in the AP profile and/or VGCC gating properties can alter AP-driven Ca^{2+} signaling. This is of potential physiological relevance for many cell types, in which receptor activation is frequently accompanied by changes in the pattern of AP firing. For example, in immortalized gonadotropin-releasing hormone (GnRH)-secreting neurons (GT1 cells), activation of endogenous phospholipase C-coupled GnRH receptors stimulates a voltage-independent Ca^{2+} current that depolarizes the baseline potential reached during the interpulse interval. This increases the frequency of firing and shifts the profile of the AP waveform from sharp, high-amplitude spikes (hereafter sharp spikes) to broad, low-amplitude spikes (hereafter broad spikes) (Van Goor et al., 1999a,b). Activation of thyropropin-releasing hormone or corticotropin-releasing hormone receptors also depolarizes the baseline potential, which leads to a similar shift in the pattern of firing in pituitary lactotrophs and corticotrophs, respectively (Sankaranarayanan and Simasko, 1996; Kuryshev et al., 1997).

However, the relationship between the profile of the AP waveform and voltage-gated Ca^{2+} influx and the ionic mechanisms mediating agonist-induced spike broadening in neuroendocrine cells have been incompletely characterized. For example, experimental (McCobb and Beam, 1991; Toth and Miller, 1995) and theoretical (Augustine, 1990) findings indicate that spike broadening increases peak I_{Ca} because of an increase in the probability of the channels being in the open state. In contrast, spike broadening has been found to decrease the peak I_{Ca} in some neurons (Park and Dunlap, 1998). A reduction in spike amplitude has also been demonstrated to decrease the peak I_{Ca} (Toth and Miller, 1995) and associated Ca^{2+} entry (Callaway and Ross, 1995; Spruston et al., 1995), reflecting the activation of fewer channels. In addition, several potential mechanisms could mediate agonist-induced spike broadening. One possibility is that agonist-induced activation of intracellular signaling pathways may inhibit voltage-gated K^+ currents (I_K) to stimulate spike broadening (Goldsmith and Abrams, 1992). Alternatively, membrane depolarization and the ensuing increase in spike frequency may inactivate I_K and slow AP repolarization (Jackson et al., 1991). Finally, the decrease in spike amplitude in response to agonist-induced membrane depolarization may activate less I_K and thus cause spike broadening and change the pattern of AP-driven Ca^{2+} entry

Received for publication 3 November 1999 and in final form 5 June 2000.

Address reprint requests to Dr. Fredrick Van Goor, Endocrinology and Reproduction Research Branch, National Institute of Child Health and Human Development, National Institutes of Health, Building 49, Room 6A36, Bethesda, MD 20892-4510. Tel.: 301-496-8164; Fax: 301-480-8010; E-mail: fredrick@box-f.nih.gov.

0006-3495/00/09/1310/14 $2.00

and the associated increase in intracellular Ca^{2+} concentration ($[Ca^{2+}]_i$).

In this study, we first examined the ionic mechanism mediating depolarization-induced spike broadening in GT1 neurons, using prerecorded sharp and agonist-induced broad AP waveforms as the voltage command. The use of prerecorded AP waveforms allows for the physiological characterization of the ionic currents underlying the generation of different AP waveform subtypes. The validity of our experimental findings was tested by comparing them with a computational model that was based exclusively on the properties of the individual ionic currents characterized in GT1 neurons. We next examined the impact of the shift in the AP profile on I_{Ca} to determine why Ca^{2+} influx is enhanced despite the decrease in spike amplitude during sustained membrane depolarization. Finally, we used the GT1 cell model to examine the influence of VGCC gating properties on the ability of AP broadening to enhance the I_{Ca}.

MATERIALS AND METHODS

GT1 cell culture

All experiments were performed on the GT1-7 subtype of immortalized GnRH neurons (Mellon et al., 1990), which were originally provided by Richard I. Weiner (University of California, San Francisco). The cells were grown in 75-ml culture flasks containing culture medium composed of Dulbecco's minimum essential medium/F-12 (1:1) with L-glutamate, pyridoxine hydrochloride, 2.5 g/liter sodium bicarbonate, 10% heat-inactivated fetal bovine serum, and 100 μg/ml gentamicin (GIBCO, Grand Island, NY). At confluence, the cells were dispersed by trypsinization (0.05% trypsin) for 10 min, resuspended in culture medium, and plated on poly-L-lysine-coated (0.01%) coverslips (50,000 cells/ml) in 35-mm tissue culture dishes (Corning, Corning, NY). After incubation for 48 h, the culture medium was replaced with medium containing B-27 serum-free supplement (GIBCO) to induce morphological differentiation of the cells. All experiments were performed 3–5 days after serum removal.

Electrophysiological recordings

With the exception of I_{Ca} recordings, all ionic currents and membrane potentials (V_m) were measured with the perforated-patch recording technique (Rae et al., 1991). For the recording of I_{Ca}, regular whole-cell recording techniques were used (Van Goor et al., 1999b). Current-clamp and voltage-clamp recordings were performed at room temperature with an Axopatch 200 B patch-clamp amplifier (Axon Instruments, Foster City, CA) and were low-pass filtered at 2 kHz. For perforated-patch recordings, the patch pipette tips (3–5 MΩ) were briefly immersed in amphotericin B-free solution and then back-filled with amphotericin B (240 μg/ml)-containing solution. Before seal formation, liquid junction potentials were canceled. An average series resistance of 17 $\pm$ 1 MΩ was reached 10 min after the formation of a gigaohm seal (seal resistance $>$ 5 GΩ) and remained stable for up to 1 h. When necessary, series resistance compensation was optimized. Capacitive current was reduced by coating the pipette tips with Sylgard (Dow Corning Corporation, Midland, MI) and by maintaining low bath solution levels. The remaining capacitive current was removed by using the capacity compensation circuitry of the patch-clamp amplifier. An average membrane capacitance (C_m) of 10 $\pm$ 1 pF (n = 41) was determined using the membrane test function in Clampex 8 (Axon Instruments). Pulse generation, data acquisition, and analysis were done with a PC equipped with a Digidata 1200 A/D interface in conjunction with Clampex 8 (Axon Instruments). All values in the text are reported as means $\pm$ SEM. In some cases, the current-voltage relations were fit with a single Boltzmann relation: $I/I_{max} = 1/(1 + \exp((E - E_{1/2})/k))$, where I_{max} is the maximum inward current, E is the prepulse potential, $E_{1/2}$ is the V_m at which there is 50% of the maximum current, and k is the slope factor. Differences between groups were considered to be significant when $p < 0.05$ with the paired t test.

Measurement of $[Ca^{2+}]_i$

GT1 neurons were incubated for 15 min at 37°C in phenol red-free medium 199 containing Hanks' salts, 20 mM sodium bicarbonate, 20 mM HEPES, and 0.5 μM indo-1 AM (Molecular Probes, Eugene, OR). The coverslips with cells attached were then washed twice with modified Krebs-Ringer's solution containing (in mM) 120 NaCl, 4.7 KCl, 2.6 $CaCl_2$, 2 $MgCl_2$, 0.7 $MgSO_4$, 10 HEPES, and 10 glucose (pH adjusted to 7.4 with NaOH) and mounted on the stage of an inverted epifluorescence microscope (Nikon). A Nikon photon counter system was used to simultaneously measure the intensity of light emitted at 405 nm and at 480 nm after excitation at 340 nm. Background intensity at each emission wavelength was corrected. Perforated patch recording techniques (see above) were used to control the V_m and to inject the different AP waveforms to measure AP-driven Ca^{2+} entry. The data were digitized at 4 kHz, using a PC equipped with the Clampex 8 software package in conjunction with a Digidata 1200 A/D converter (Axon Instruments). The $[Ca^{2+}]_i$ was calibrated in vivo according to the method of Kao (1994). Briefly, R_{min} was determined by exposing the cells to 10 μM Br-A23187 in the presence of Krebs-Ringer's solution with 2 mM EGTA and 0 Ca^{2+} for 60 min; 15 mM Ca^{2+} was then added to determine R_{max}. The values used for R_{min}, R_{max}, $S_{f,480}/S_{b,480}$, and K_d were 0.472, 3.634, 3.187, and 230 nM, respectively.

Chemicals and solutions

Stock solutions of tetrodotoxin (TTX) citrate (Research Biochemicals International, Natick, MA) were prepared in double-distilled, deionized water. Stock solutions of nifedipine and S(−)-Bay K 8644 (Research Biochemicals International) were prepared in dimethylsulfoxide and ethanol, respectively. The maximum final concentrations of dimethylsulfoxide and ethanol were 0.1% and 0.01%, respectively, neither of which altered the electrical membrane activity of ionic currents.

For the recording of electrical activity and total inward and outward currents, the extracellular medium contained modified Krebs-Ringer salts, and the pipette solution contained (in mM) 70 KCl, 70 K-aspartate, 1 $MgCl_2$, and 10 HEPES (pH adjusted to 7.2 with KOH). To isolate voltage-dependent Na^+ currents (I_{Na}), the extracellular medium contained Krebs-Ringer's solution without $CaCl_2$ and with 20 mM tetraethylammonium (TEA), 5 mM 4-AP, and 50 μM $CdCl_2$, and the pipette contained (in mM) 70 CsCl, 70 Cs-methanesulfonate, 2 $MgCl_2$, and 10 HEPES (pH adjusted to 7.2 with CsOH). To isolated I_{Ca}, conventional whole-cell recording techniques were used as previously described (Van Goor et al., 1999b). The extracellular medium contained Krebs-Ringer's solution with 20 mM TEA, 2.6 mM or 10 mM $CaCl_2$, and 1 μM TTX (pH adjusted to 7.4 with NaOH). The pipette solution contained (in mM) 120 CsCl, 20 TEA-Cl, 4 $MgCl_2$, 10 EGTA, 9 glucose, 20 HEPES, 0.3 Tris-GTP, 4 Mg-ATP, 14 $CrPO_4$, and 50 U/ml creatine phosphokinase (pH adjusted to 7.2 with Tris base). Under these recording conditions, the I_{Ca} was further isolated by subtracting the current evoked in the presence of 100 μM $NiCl_2$ and 200 μM $CdCl_2$ from the total current. All I_{Ca} recordings shown and analyzed were of the Ni^{2+}- and Cd^{2+}-sensitive current. To isolate I_K, the extracellular medium contained Krebs-Ringer's solution without $CaCl_2$ and with 1 μM TTX, and the pipette contained (in mM) 70 KCl, 70 K-aspartate, 1 $MgCl_2$, and 10 HEPES (pH adjusted to 7.2 with KOH). All reported V_m measurements made under total current and I_K recording conditions were corrected for a liquid junction potential of +10 mV between the pipette and bath solution

(Barry, 1994). The V_m under I_{Na} recording conditions was corrected for a liquid junction potential of +7 mV. No correction was required under isolated I_{Ca} recording conditions. The bath contained <500 μl of saline that was continuously replaced at a rate of 2 ml/min with a gravity-driven perfusion system. The inflow was placed adjacent to the cell, resulting in complete solution exchange around the cell within 2 s. A solid Ag/AgCl reference electrode was connected to the bath via a 3 M KCl agar bridge.

Model description

To provide a rigorous quantitative test of the experimental data, we developed a mathematical model in which the properties of the ionic currents used were determined directly from square-wave pulse voltage-clamp data. The ionic currents used included a TTX-sensitive I_{Na}, L- and T-type I_{Ca}, a voltage-sensitive (delayed-rectifier-type) I_K, an M-like I_K (I_M), and an inward rectifier I_K (I_{ir}). Furthermore, there is a Ca^{2+}-permeable, voltage-insensitive inward leak current that offsets the I_{ir} (the major I_K active during the interspike period) to maintain repetitive firing. Although GT1 cells express large- and small-conductance Ca^{2+}-activated K^+ currents (Spergel et al., 1996; Van Goor et al., 1999a), the $[Ca^{2+}]_i$ levels reached during spontaneous AP firing are not sufficient to activate them and were therefore omitted. All of the currents, except I_{Na}, are described by typical Hodgkin-Huxley equations (Hodgkin and Huxley, 1952), including voltage-regulated activation and inactivation gating variables, macroscopic ionic conductances, and linear driving forces. The parameters and precise forms of the equations, as well as other model parameters, were obtained directly from our experimental recordings in GT1 cells (Van Goor et al., 1999b, and unpublished observations). Full model equations and parameter values are given in the Appendix.

In the development of a model system describing the electrical membrane activity in GT1 neurons, a Hodgkin-Huxley-like description of the TTX-sensitive I_{Na} was initially used. In this description, I_{Na} exhibited a large surge of activation during the spike repolarization (data not shown), which was never observed experimentally. Simulated V_m depolarization also did not induce spike broadening (data not shown), suggesting that the gating kinetics for the I_{Na} in this description do not accurately reflect those in GT1 neurons. In the Hodgkin-Huxley-like description, it is assumed that activation and inactivation are independent processes and that both are voltage dependent (Hodgkin and Huxley, 1952). However, it has long been known that this is not the case for TTX-sensitive Na^+ channels (Bezanilla and Armstrong, 1977; Aldrich et al., 1983; Kuo and Bean, 1994). Instead, inactivation is linked to activation and may not be intrinsically voltage dependent, deriving its apparent voltage dependence from the linkage with activation. In addition, Kuo and Bean (1994) showed that Na^+ channels must deactivate fully before they can recover from inactivation.

Consequently, we adapted Kuo and Bean's (1994) model of I_{Na} in rat hippocampal CA1 neurons for the GT1 neuronal I_{Na} to fit the experimental data. In particular, the slow recovery from inactivation of the I_{Na} (>500 ms; Van Goor et al., 1999b) was incorporated into the description of the I_{Na} in the GT1 cell model. In this description, the Na^+ channel is composed of subunits with four possible states: deactivated (D), activated (A), deactivated-inhibited (D*), and activated-inhibited (A*) (see the reaction scheme in the Appendix for further details). A channel consists of three such subunits, meaning that there are 64 possible states overall. As a whole, however, the channel can be considered to be in one of three states. The conducting (open) state is denoted O and is given solely by A^3; the channel is inactivated (I) if any of the three subunits is in either inhibited state. All other modes represent the closed (C) state.

RESULTS

Depolarization-induced shift in AP firing patterns

It has been shown that activation of endogenous Ca^{2+}-mobilizing receptors in GT1 neurons induces sustained depolarization in the baseline V_m, which shifts the pattern of AP firing from sharp to broad spikes (Fig. 1 *A*; Van Goor et al., 1999a,b). In this study, both experimental and theoretical approaches were used to determine if depolarization of the baseline V_m in the absence of receptor activation could also shift the profile of the AP waveform. To do this, GT1 cells were depolarized by the application of positive current injections. This should mimic the effects of agonist-induced V_m depolarization, but not those resulting from the activation of intracellular messengers other than Ca^{2+}. In nine separate cells, 15-pA current injection (Fig. 1 *B*) depolarized the V_m by 9 ± 1 mV, which is similar to that observed in GnRH-stimulated cells (9 ± 1 mV, n = 15; Van Goor et al., 1999a,b). Depolarization of the V_m by current injection

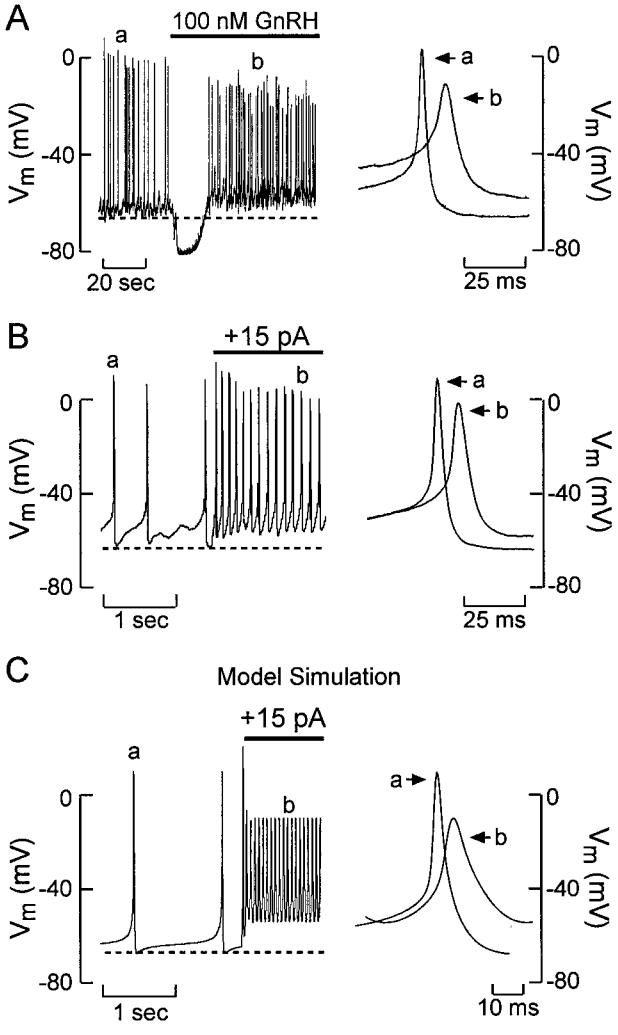

FIGURE 1 Depolarization-induced shift from sharp to broad spikes in GT1 neurons. (*A* and *B*) Representative V_m traces of the response to application of 100 nM GnRH (*A*, *bar*) or +15 pA current injection (*B*, *bar*). (*C*) Simulation of depolarizing current injection (*bar*) in the GT1 cell model. Expanded time scales for the APs identified by *a* and *b* in *A–C* (*left*) are shown in the right panels. The dotted lines represent the baseline V_m.

also mimicked the action of GnRH on firing frequency and the profile of the AP waveform (Fig. 1 *A* versus Fig. 1 *B*). In particular, depolarization of the baseline potential by 15-pA current injections increased the firing frequency from 0.6 ± 0.2 Hz to 1.3 ± 0.2 Hz ($n = 9$, $p < 0.05$). In addition, the peak AP amplitude decreased from 0.4 ± 1.6 mV to −14.5 ± 1.0 mV, and the AP duration at one-half amplitude increased from 6.7 ± 0.3 ms to 18.8 ± 2.5 ms (mean ± SEM; $p < 0.05$; $n = 9$). In the GT1 cell model, simulation of depolarizing current injections also shifted the firing pattern from sharp to broad spikes (Fig. 1 *C*). These results indicate that sustained depolarization of the baseline V_m is sufficient to mimic the agonist-induced shift in the profile of the AP waveform from sharp to broad spikes.

Voltage-gated ionic currents contributing to sharp and broad firing patterns

The ionic currents underlying the generation of the different AP waveforms in GT1 neurons were analyzed using the AP clamp technique. Prerecorded spike trains from before (sharp spike train) and after (broad spike train) non-receptor-mediated membrane depolarization were used as the command potential in the voltage-clamp recording mode (Fig. 2). The interspike interval of the sharp spike train was characterized by a pacemaker depolarization that initiated at a baseline V_m of −66.7 ± 0.3 mV and culminated in spike initiation at a threshold of −50.7 ± 0.7 mV (Fig. 2 *A*, *left*). The rapid upstroke of the AP had a rise rate of 19.3 ± 2.4 mV/ms and reached a peak potential of 13.0 ± 1.5 mV. Repolarization was also rapid (16.0 ± 2.0 mV/ms), limiting spike duration measured at half-amplitude to 4.2 ± 0.2 ms. For the broad spike train, the pacemaker depolarization was initiated at −56.3 ± 0.7 mV and culminated in spike initiation at a threshold of −46.3 ± 0.9 mV. Compared to the sharp AP, the upstroke had a slower rise rate (3.7 ± 0.3 mV/ms) and a lower peak potential (−8.0 ± 1.0 mV; Fig. 2 *A*, *right*). Repolarization was also slower (5.3 ± 0.3 mV/ms), resulting in a longer duration of AP (19.3 ± 1.1 ms). Under total current recording conditions in the voltage-clamp mode, both the sharp and broad spike trains activated an inward current followed by an outward current (Fig. 2 *B*). The net inward current increased rapidly during the spike upstroke, whereas the net outward current predominated during the repolarization phase (Fig. 2 *C*).

The ionic currents underlying the generation of the sharp and broad AP waveforms in GT1 neurons were also analyzed using the GT1 cell model (Fig. 3 *A*). As observed under experimental conditions, a net inward current generated the upstroke of both the sharp and broad AP waveforms. This was followed by the development of a net outward current that repolarized the cells (Fig. 3, *B* and *C*). These experimental and theoretical results indicate that the depolarization-induced shift in the AP waveform is due to the inherent properties of the individual ionic currents expressed in GT1 neurons.

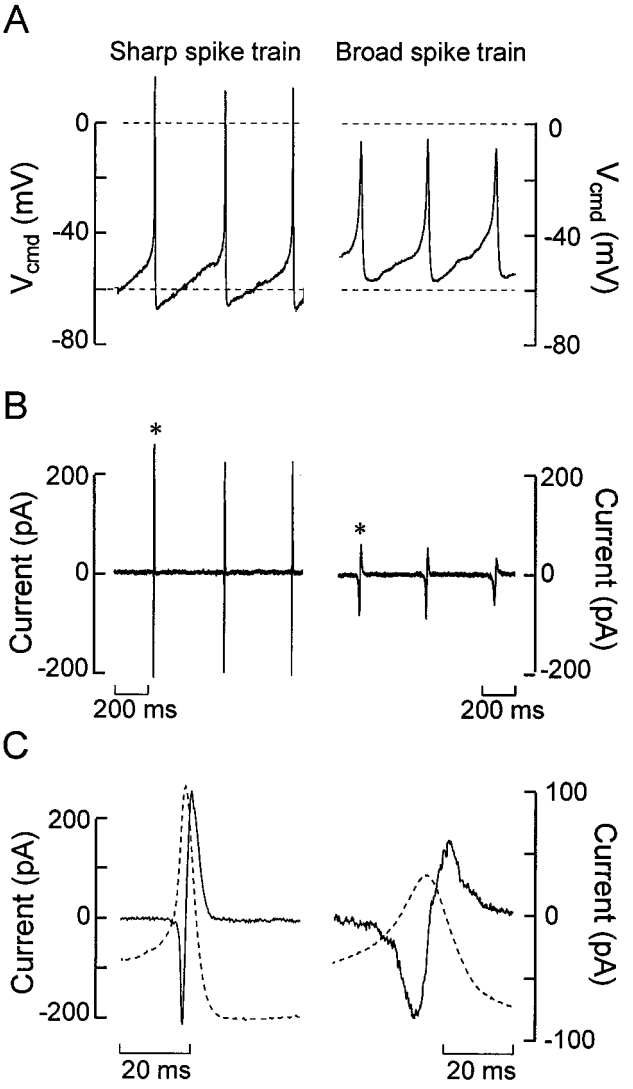

FIGURE 2 Total ionic current evoked by prerecorded sharp and broad spike train command potentials in GT1 neurons. (*A*) Typical example of the AP firing patterns before (sharp spike train) and after (broad spike train) agonist-induced V_m depolarization. (*B*) Total ionic current evoked by the sharp and broad spike trains in the voltage-clamp mode from the same cell. (*C*) Expanded time scale of spikes (- - - - -) and the evoked currents (——) identified by the asterisks in *B*. The V_m recordings shown in *A* were used as the broad and sharp spike train command potentials under all subsequent experimental conditions.

Dependence of spiking pattern on voltage-gated I_{Na}

The physiological roles of I_{Na} in the generation of sharp and broad AP waveforms were analyzed under isolated I_{Na} recording conditions as described in Materials and Methods. Under these conditions, both the sharp and broad spike

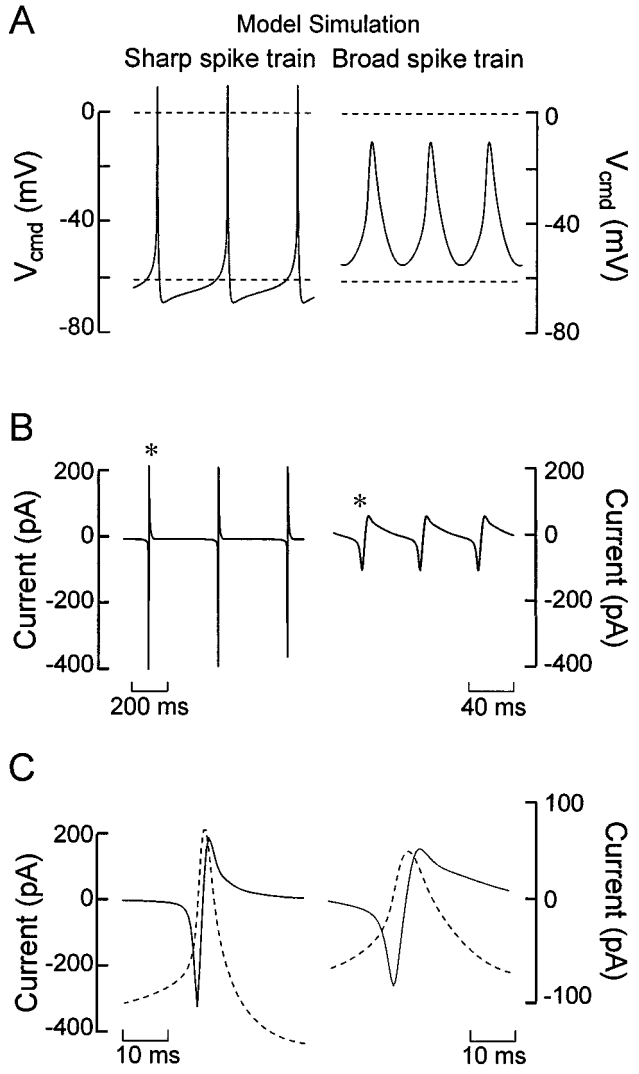

FIGURE 3 Simulations of the total ionic current evoked by sharp and broad spike train command potentials in the GT1 cell model. (*A*) The AP firing patterns before (sharp spike train) and after (broad spike train) the simulation of agonist-induced V_m depolarization. (*B*) Total ionic current underlying the generation of sharp and broad spike trains. (*C*) Expanded time scale of spikes (- - - - -) and the underlying currents (——) identified by the asterisks in *B*.

trains evoked an inward current that was abolished by TTX, a specific blocker of voltage-gated I_{Na} (Fig. 4, *A* and *B*). The sharp spike train evoked a transient inward current at V_m more depolarized than -50 ± 1 mV ($n = 12$), which was near the spike initiation threshold in these cells (Fig. 4 *A*, *left*). The I_{Na} reached a peak amplitude of -213 ± 17 pA, then decreased rapidly because of inactivation and deactivation (Fig. 4 *C*, *left*). Most of the I_{Na} was observed during the sharp upstroke of the AP, but a small amount was observed during the repolarization phase (Fig. 4 *C*, *left*) and may correspond to the resurgent I_{Na} in other neurons (Raman and Bean, 1997, 1999). The broad spike train also activated a transient I_{Na} at V_m more depolarized than -47 ± 1 mV ($n = 12$). The mean amplitude of this current (-25 ± 3 pA, $n = 12$; Fig. 4 *A*, *right*) was much smaller than that evoked by the sharp spike train (Fig. 4, *A* and *C*). Although a majority of the I_{Na} was activated during the upstroke of the broad spikes, small amounts of current were also observed during the sustained pacemaker depolarization and the repolarization phase (Fig. 4 *C*, *right*). The GT1 cell model mimicked these experimental observations when Kuo and Bean's (1994) description of I_{Na} was used (Fig. 4 *D*).

Based on the conventional square waveform voltage-step protocols, we previously suggested that the reduction in AP amplitude during agonist-induced V_m depolarization reflected the steady-state inactivation of the I_{Na}. To test this hypothesis more directly, the steady-state inactivation of the spike-induced I_{Na} was examined using a modified two-pulse protocol. Cells held at -67 mV were subjected to 1.5-s conditioning prepulses from -87 mV to -37 mV before the application of a single sharp spike (Fig. 5 *A*, *left*). The peak I_{Na} evoked during the spike was then plotted against the conditioning prepulse and fitted with a Boltzmann relation, where $E_{1/2}$ and k (see Materials and Methods) were -61.3 mV and 5.6 mV, respectively (Fig. 5 *A*, *right*). The sharp decline in peak I_{Na} between -80 mV and -50 mV indicates that small degrees of depolarization of the baseline potential are sufficient to limit I_{Na} participation during spike generation. This is consistent with the smaller peak I_{Na} amplitude activated by the broad spike train than that activated by the sharp spike train.

The reason for the decrease in I_{Na} amplitude in response to sustained V_m depolarization is illustrated by the relative proportions of the Na^+ channel states during AP activity derived from the GT1 cell model (Fig. 5 *B*). For sharp spikes (Fig. 5 *B*, *left*), ~60% of the channels are available to be activated before spike initiation, the remainder being in the inactivated state. During the spike, less than 10% of the sodium channels are in the conducting state, as most become inactivated and recover slowly to the closed state. In depolarized cells firing broad spikes (Fig. 5 *B*, *right*), more than 90% of the channels are in the inactivated state before spike initiation. Consequently, the fraction of available sodium channels is small, which is reflected by the small I_{Na} evoked during the spike upstroke (Fig. 4 *D*). Together with the experimental data, these results demonstrate that sustained V_m depolarization inactivates I_{Na} to reduce spike amplitude in GT1 neurons.

Dependence of spiking pattern on voltage-gated I_K

We next examined the possibility that the decrease in spike amplitude caused by inactivation of I_{Na} during sustained baseline V_m depolarization limits I_K activation to promote spike broadening. Under isolated I_K recording conditions

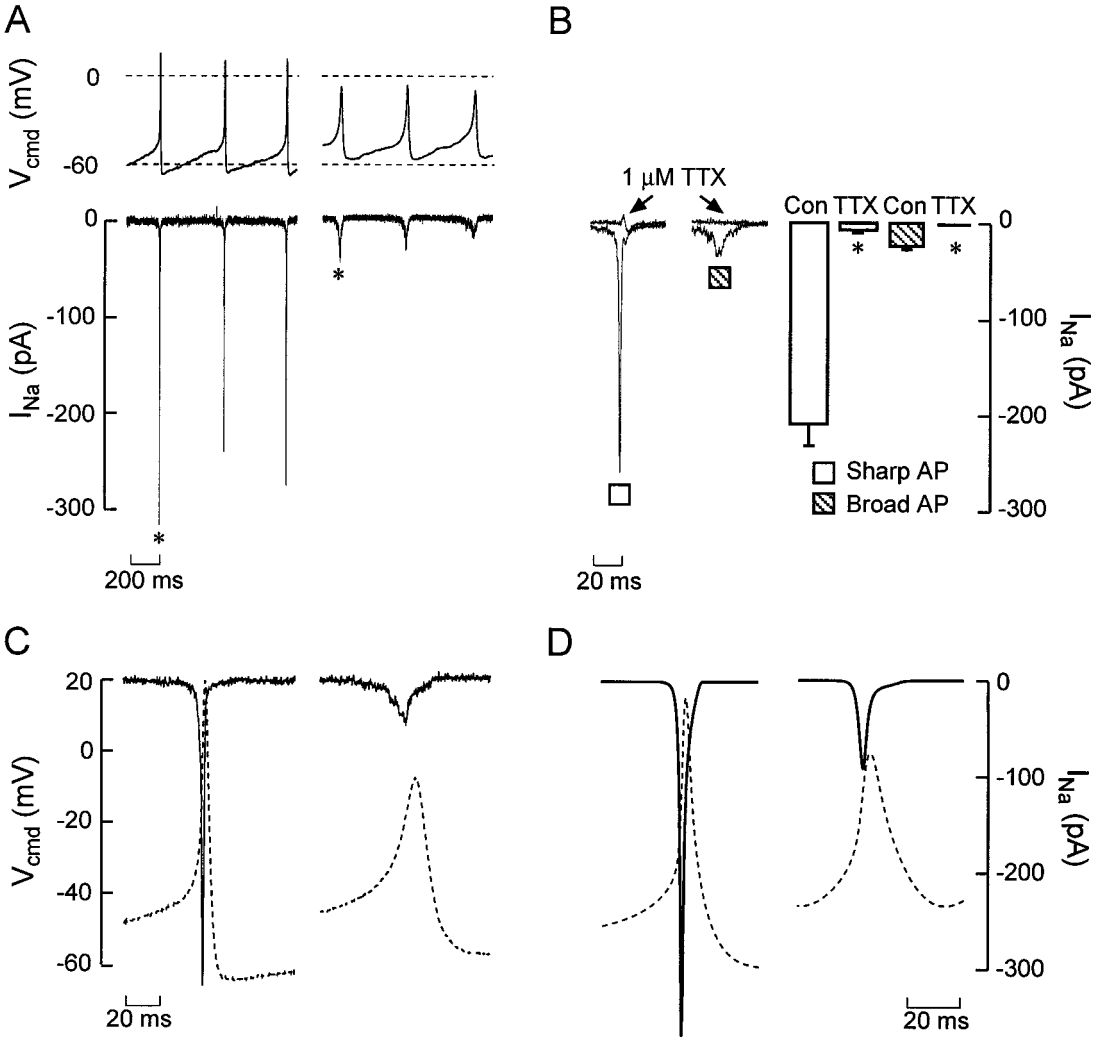

FIGURE 4 The contribution of TTX-sensitive I_{Na} to the generation of sharp and broad spike trains in GT1 neurons. (*A*) Representative current trace of the isolated I_{Na} (*bottom*) evoked by the sharp (holding potential = −67 mV) and broad (holding potential = −51 mV) spike trains (*top*) in the same cell. (*B*) (*Left*) Representative I_{Na} traces evoked by sharp (□) and broad (▨) spike trains in the absence and presence (*arrows*) of 1 μM TTX in the same cell. For clarity, only the currents evoked during the middle spikes were shown. (*Right*) Effects of 1 μM TTX on the I_{Na} evoked by the spike train command potentials (mean ± SEM, $n = 5$). Asterisks denote significant differences compared with control values: $p < 0.01$, paired *t*-test. (*C*) Expanded time scales of the spike trains (- - - - -) and the evoked I_{Na} (——) identified by the asterisks in *A*. (*D*) Simulation of the I_{Na} (——) underlying the generation of sharp and broad AP waveforms (- - - - -) in the GT1 cell model.

(see Materials and Methods), both the sharp and broad spike trains evoked an outward current that was reduced by the application of 2 mM tetraethylammonium (TEA) (Fig. 6 *A* and *B*). However, the peak TEA-sensitive I_K evoked by the broad spike train was much lower than that evoked by the sharp spike train (Fig. 6 *C*). The peak I_K amplitudes during the sharp and broad spike trains were 300 ± 28 pA and 107 ± 17 pA, respectively ($n = 12$; $p < 0.01$). In the GT1 cell model, the behavior of the I_K was similar to that observed experimentally. In particular, the I_K underlying the generation of sharp spikes was of much greater amplitude than that observed during broad spikes (Fig. 6 *D*).

Under both experimental and theoretical conditions, the I_K began to activate during the latter part of the spike upstroke. Most of the I_K, however, was observed during the falling phase of both waveform subtypes (Fig. 6, *C* and *D*). The impact of I_K on the rate of V_m repolarization (dV_m/dt) at a given time point was calculated by dividing the I_K by the C_m. Using a mean C_p of 10 ± 1 pF ($n = 41$) and the peak I_K evoked by sharp or broad spike trains, the maximum calculated rates of V_m repolarization due to I_K activation for each waveform were 30 mV/ms and 10.7 mV/ms, respectively. These results demonstrate that TEA-sensitive I_K mediates the rate of V_m repolarization during both sharp and broad AP firing patterns in GT1 neurons. They also indicate that spike amplitude, which is determined by the availability of I_{Na} before spike initiation, controls the rate of V_m repolarization by determining the amount of I_K activation.

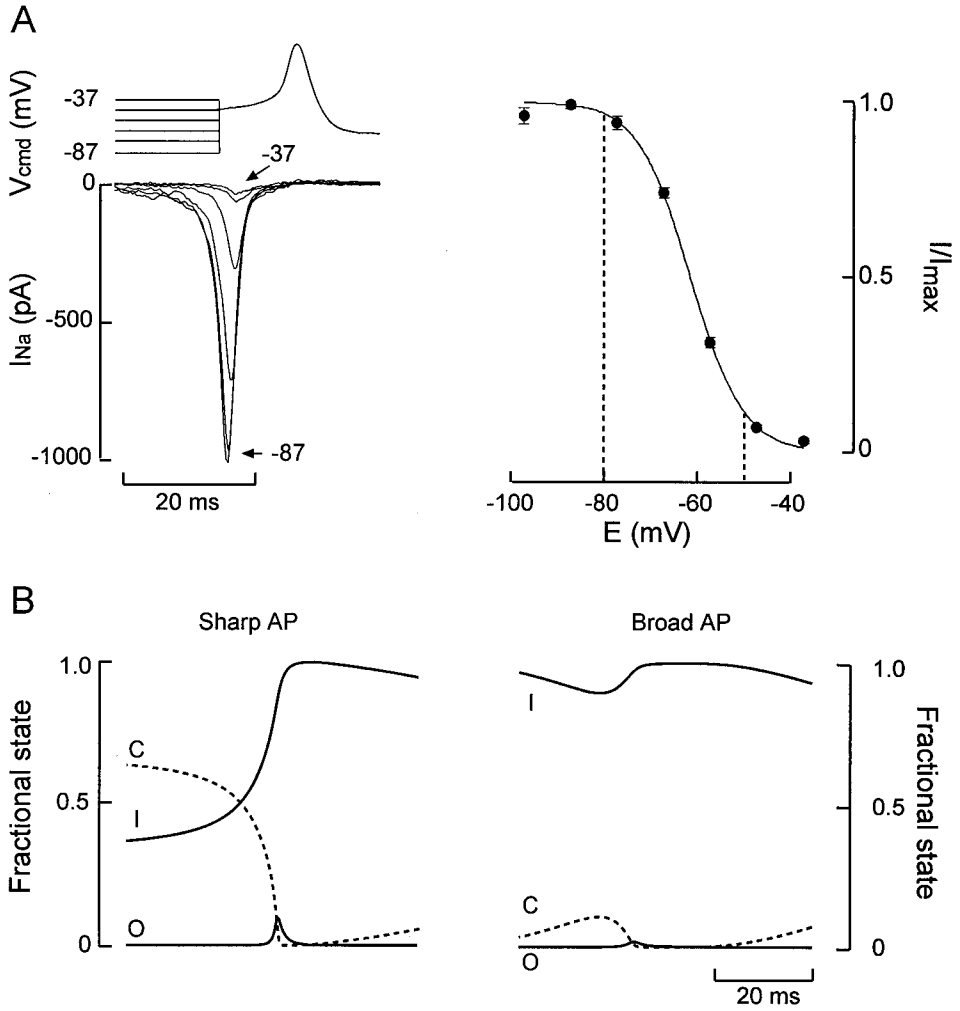

FIGURE 5 Depolarization-induced inactivation leads to the reduction in I_{Na} amplitude during the broad spike train. (*A*) Steady-state inactivation of the I_{Na} evoked by a single sharp spike in GT1 neurons. The steady-state inactivation curves for the I_{Na} were generated from prepulse experiments in which the V_m was stepped from −87 mV to −37 mV for 1.5 s before the application of the AP waveform (holding potential = −87 mV). (*Left*) Representative traces of the I_{Na} evoked by the spike train after prepulse potentials between −87 and −37 mV. (*Right*) Steady-state inactivation curve of the I_{Na} (mean ± SEM; $n = 5$). The current was normalized to the maximum inward current and fitted with a single Boltzmann relation. The dashed lines indicate the range of baseline V_m observed in spontaneously active GT1 neurons. (*B*) The time course of the open (O), inactivated (I), and closed (C) states of the I_{Na} during the firing of sharp and broad AP waveforms.

Dependence of voltage-gated Ca^{2+} entry on the pattern of firing

To examine the impact of spike broadening on voltage-gated Ca^{2+} entry, we monitored the I_{Ca} evoked by the sharp and broad AP waveforms under isolated I_{Ca} recording conditions as described in Materials and Methods. In 15 individual cells, application of both sharp and broad spike trains evoked rapid increases in inward I_{Ca} that peaked during the initial phases of spike repolarization (Fig. 7, *A* and *B*). The occurrence of the peak I_{Ca} during the repolarization phase is presumably due to the increase in driving force and time required for the voltage-dependent deactivation of the Ca^{2+} channel. Consistent with the role of spike amplitude in mediating voltage-gated Ca^{2+} influx, the peak I_{Ca} amplitude evoked by the broad spike train was lower than that evoked by the sharp spike train. However, despite the lower peak I_{Ca} amplitude, the integrated I_{Ca} was greater (Fig. 7, *B* and *C*). In the GT1 cell model, the behavior of the I_{Ca} was similar to that observed experimentally. In particular, despite the decrease in peak I_{Ca} amplitude, the integrated I_{Ca} was greater during the broad spike train compared to the sharp spike train (Fig. 7 *D*).

In further studies, we characterized the ionic and pharmacological characteristics of the I_{Ca} evoked by the prerecorded spike trains. In 15 individual cells, increasing the extracellular Ca^{2+} concentration from 2.6 to 10 mM augmented the peak I_{Ca} evoked by both sharp (from 135 ± 15 pA to 256 ± 37 pA) and broad (from 103 ± 11 pA to 161 ± 29 pA) AP waveforms. Moreover, the ability of the broad AP waveform to drive more Ca^{2+} per spike into the cell was maintained in the presence of 10 mM extracellular Ca^{2+} (Fig. 8 *A*). Application of the VGCC antagonist nifedipine reduced the integrated I_{Ca} evoked by both AP waveform subtypes (Fig. 8 *B*). In contrast, the VGCC activator Bay K 8644 increased the integrated I_{Ca} evoked by both the sharp and broad AP waveforms (Fig. 8 *B*). Thus, depolarization-induced spike broadening increases the integrated I_{Ca} through L-type Ca^{2+} channels.

To examine the dependence of voltage-gated Ca^{2+} entry on the profile of the AP waveform, we measured the in-

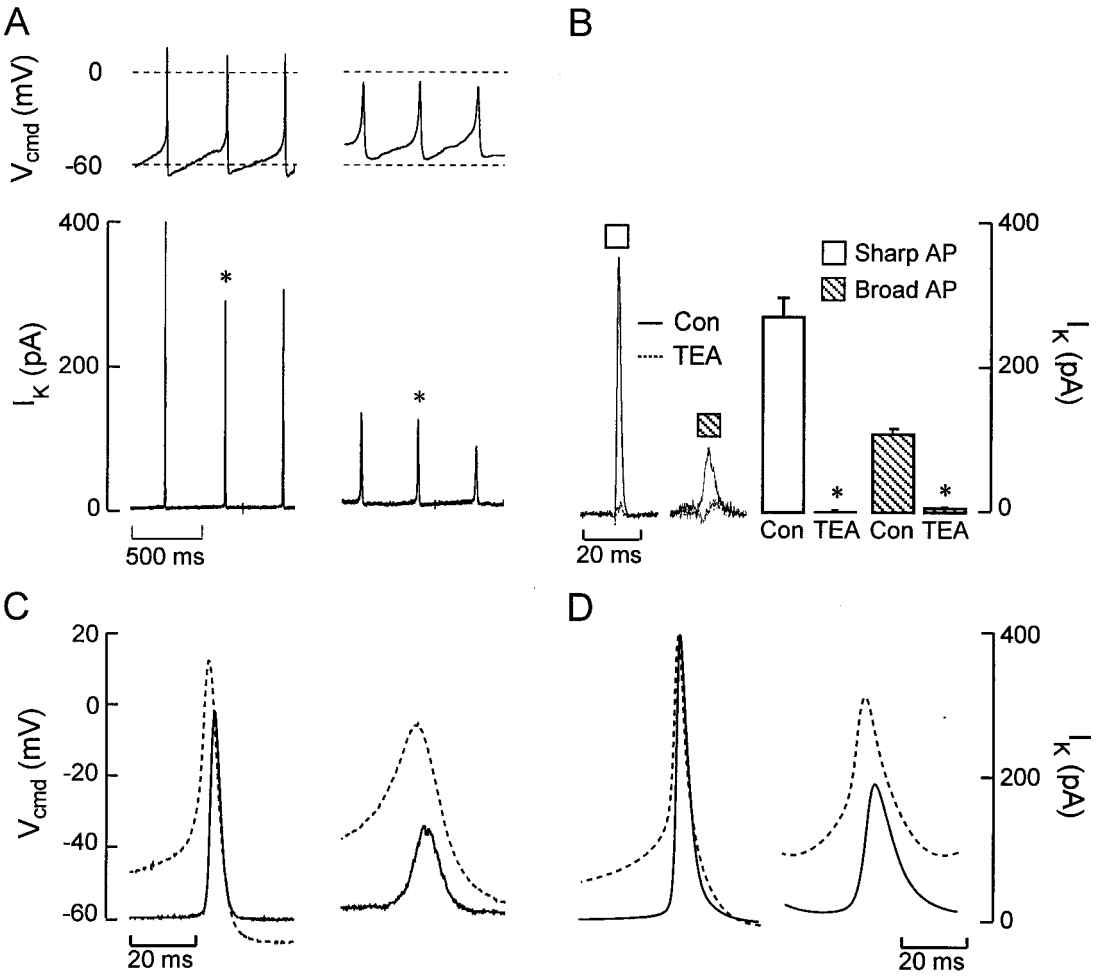

FIGURE 6 Voltage-gated I_K evoked by sharp and broad spike trains in GT1 neurons. (*A*) Isolated I_K (*bottom*) evoked by the sharp and broad spike train command potentials (*top*) in the same cell. (*B*) (*Left*) Representative I_K traces evoked by sharp (□) and broad (▨) spike trains in the absence (——) and presence (- - - - -) of 2 mM TEA in the same cell. For clarity, only the currents evoked during the middle spikes were shown. (*Right*) Effects of 2 mM TEA on the I_K evoked by the spike train command potentials (mean ± SEM, $n = 5$). Asterisks in *B* indicate significant differences compared with control values: $p < 0.01$, paired *t*-test. (*C*) Expanded time scale of the spike trains (- - - - -) and the evoked I_K (——) identified by the asterisks in *A*. (*D*) Simulation of the I_K (——) underlying the generation of sharp and broad AP waveforms (- - - - -) in the GT1 cell model.

crease in $[Ca^{2+}]_i$ in response to sequential application of 60 prerecorded sharp or broad APs given at a frequency of 2 Hz. Under total current recording conditions, the broad spike train increased the $[Ca^{2+}]_i$ more than the sharp spike train (Fig. 9). This increase in $[Ca^{2+}]_i$ evoked by both the sharp and broad spike trains was attenuated by application of 1 μM nifedipine and enhanced by the application of 1 μM Bay K 8644 (Fig. 9). These results are consistent with the ability of broad spike trains to drive more Ca^{2+} entry via L-type Ca^{2+} channels than the sharp spike trains.

Relationship between *I–V* characteristics and the size of I_{Ca} in firing cells

In contrast to other cell types, spike broadening in GT1 cells increases the integrated I_{Ca} despite a decrease in spike amplitude. Experimental studies indicate that both the activation threshold and peak amplitude of the dihydropyridine-sensitive I_{Ca} in GT1 neurons occur at relatively hyperpolarized membrane potentials compared to those of other cell types. We utilized the mathematical model to estimate the impact of their different *I–V* characteristics on I_{Ca} during the firing of sharp and broad APs. To do this, we shifted the half-maximum activation of the L-type Ca^{2+} channels in the hyperpolarizing or depolarizing direction (Fig. 10 *A*; see the Appendix for details). The modified *I–V* profiles were within the range observed experimentally in cells expressing different isoforms of the L-type Ca^{2+} channel; they are represented by the dashed lines in Fig. 10 *A*. The experimentally derived *I–V* relationship for the L-type Ca^{2+} channel in GT1 neurons and the corresponding I_{Ca} underlying the generation of both the sharp and broad AP waveforms

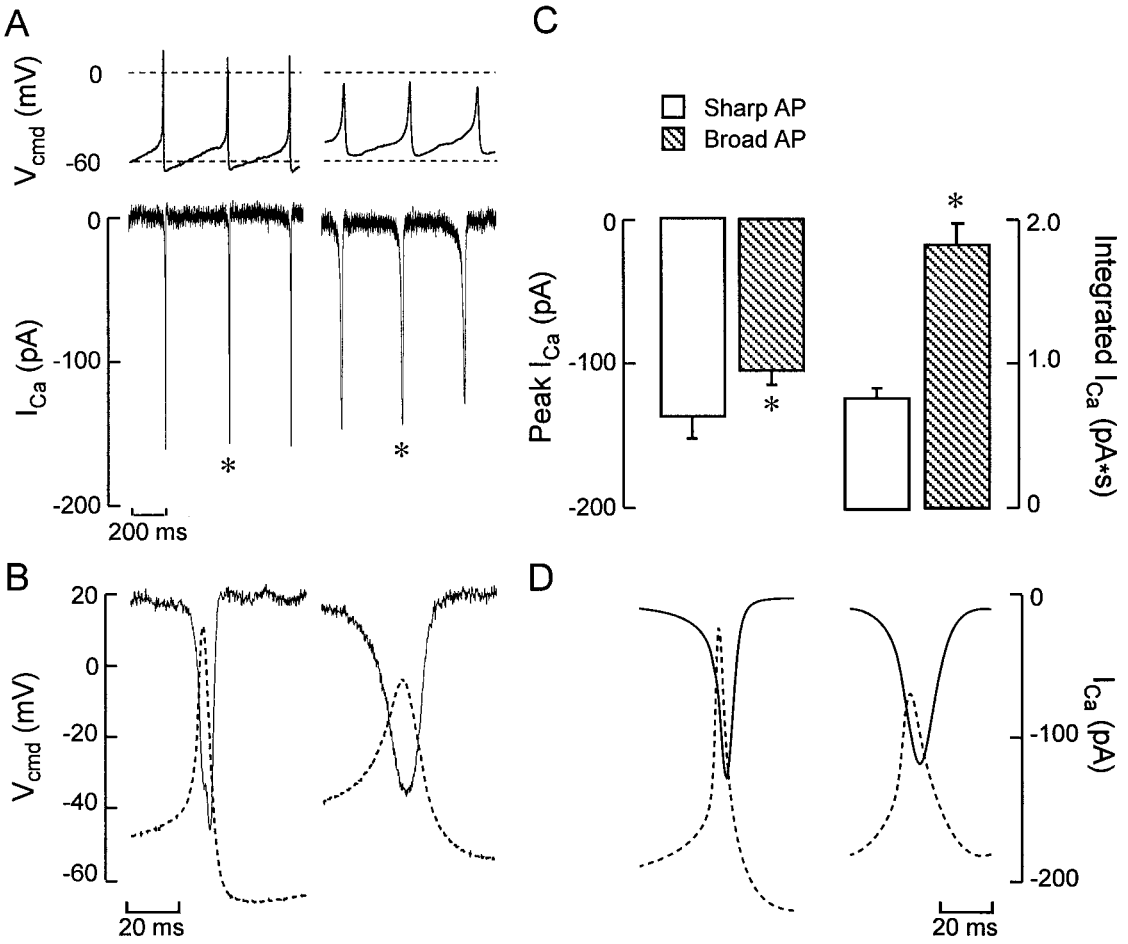

FIGURE 7 Voltage-gated I_{Ca} evoked by sharp and broad spike trains in GT1 neurons. (*A*) Isolated I_{Ca} (*bottom*) evoked by the sharp and broad spike train command potentials (*top*) in the same cell. (*B*) Expanded time scale of the spike trains (- - - - -) and the evoked I_{Ca} (——) identified by the asterisks in *A*. (*C*) Peak I_{Ca} amplitude (*left*) and integrated I_{Ca} (*right*) evoked by the sharp (□) and broad (▨) (mean ± SEM, $n = 15$) AP waveforms. Asterisks in *C* indicate significant differences compared with control values: $p < 0.01$, paired *t*-test. (*D*) Simulation of the I_{Ca} (——) underlying the generation of sharp and broad AP waveforms (- - - - -) in the GT1 cell model.

are represented by the solid lines in Fig. 10, *A* and *B*. Shifting the half-maximum activation by 10 mV in the hyperpolarizing direction increased the integrated I_{Ca} evoked by both AP waveforms (Fig. 10 *B*). However, the capacity of the broad spikes to drive more Ca^{2+} entry than the sharp spikes was reduced (Fig. 10 *C*). Incremental shifts in the half-maximum activation of the L-type Ca^{2+} channels by 10 mV in the depolarizing direction decreased the integrated I_{Ca} evoked by both AP waveforms (Fig. 10 *B*). In addition, the capacity of the broad spikes to drive more Ca^{2+} entry than the sharp spikes was reduced. Moreover, when the half-maximum activation of the I_{Ca} was depolarized beyond −20 mV, the integrated I_{Ca} underlying the generation of the sharp spike was greater than that underlying the broad spike (Fig. 10 *C*). These results indicate that the activation properties of the L-type Ca^{2+} channel isoform expressed in a particular cell type can determine the impact of spike broadening on voltage-gated Ca^{2+} entry.

DISCUSSION

Changes in the AP waveform, as observed in our studies using GT1 neurons, can occur by a number of physiological processes, and alterations in the I_{Na} and/or I_K can account for the observed effects. For example, developmental changes in Na^+ or K^+ channel density alter the profile of the AP waveform in some cell types (Gao and Ziskind-Conhaim, 1998). Similarly, the heterogeneous properties of the AP waveform in pacemaker cells from the sinoatrial node are partially due to differences in Na^+ channel density (Nathan, 1986; Irisawa et al., 1993). Regional differences in Na^+ or K^+ channel density or subtype (Westenbroek et al., 1989; Magee et al., 1998; Poolos and Johnston, 1999) also alter the AP waveform in discrete regions of the cell. In hippocampal neurons, activity-dependent I_{Na} inactivation mediates the decrease in dendritic spike amplitude and $[Ca^{2+}]_i$ during AP trains (Callaway and Ross, 1995; Spru-

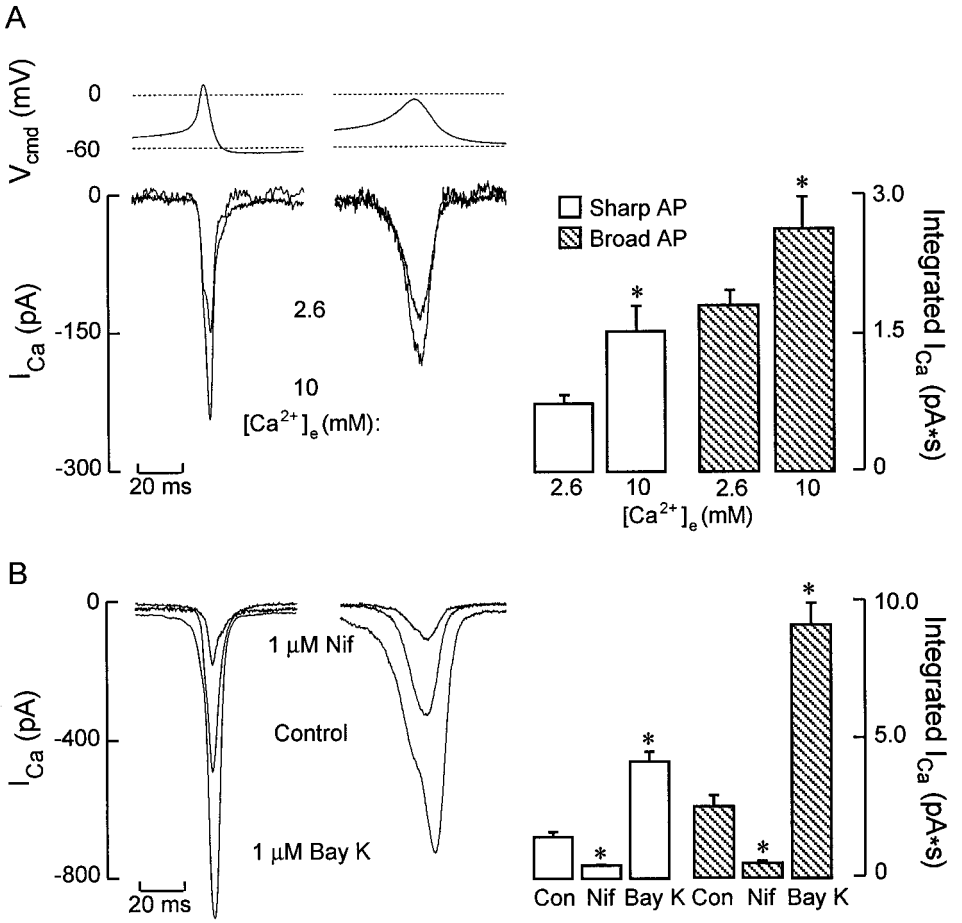

FIGURE 8 Extracellular Ca^{2+} dependence and dihydropyridine sensitivity of the I_{Ca} evoked by the sharp and broad spike trains in GT1 neurons. (*A*) (*Left*) Representative I_{Ca} traces evoked by the sharp and broad spike trains (*top*) in the presence of 2.6 mM and 10 mM extracellular Ca^{2+} in the same cell. (*Right*) Integrated I_{Ca} evoked during the sharp and broad AP waveforms in the presence of 2.6 mM and 10 mM extracellular Ca^{2+} (mean ± SEM, $n = 15$). (*B*) (*Left*) Representative I_{Ca} traces evoked by sharp and broad spike trains in the absence and presence of 1 μM nifedipine or 1 μM Bay K 8644 in the same cell. (*Right*) Effects of 1 μM nifedipine or 1 μM Bay K 8644 on the integrated I_{Ca} amplitude evoked by the sharp and broad AP waveforms (mean ± SEM, $n = 6$). For clarity, only the currents evoked during the middle spikes were shown. Asterisks indicate significant differences compared with control values: $p < 0.01$, paired *t*-test.

ston et al., 1995; Jung et al., 1997; Colbert et al., 1997). Activity-dependent inactivation of K^+ channels also alters spike duration and AP-driven Ca^{2+} entry in pituitary nerve terminals (Jackson et al., 1991). Finally, activation of intracellular messengers can modulate the activation and inactivation properties of I_{Na} and I_K to influence the pattern of AP firing (Cantrell et al., 1999; Johnston et al., 1999).

In GT1 neurons, however, the ability of non-receptor-mediated depolarization to mimic agonist application in GT1 neurons argues against the involvement of intracellular messengers in the development of spike broadening. In addition, because of the low firing frequencies observed in spontaneously active and depolarized GT1 neurons (<5 Hz), activity-dependent inactivation of I_{Na} or I_K contributes little to spike broadening (Van Goor, unpublished data). Rather, our data indicate that the inactivation properties of the TTX-sensitive I_{Na} provide a very narrow range of interpulse V_m in which the current is available for activation before spike initiation. Consequently, small degrees of depolarization of the baseline V_m by receptor-mediated or non-receptor-mediated pathways decrease the magnitude of I_{Na}, which in turn reduces the rate of rise and amplitude of the AP upstroke. This decrease in spike amplitude reduces the peak amplitude of the TEA-sensitive I_K to slow membrane repolarization, which increases spike duration and augments Ca^{2+} influx through L-type Ca^{2+} channels. Thus amplitude-dependent spike broadening facilitates AP-driven Ca^{2+} entry, which leads to the increase in $[Ca^{2+}]_i$.

Among the voltage-gated K^+ channels that may participate in AP repolarization in GT1 neurons, delayed rectifier and A-type K^+ channels have been identified in GT1 neurons (Bosma, 1993) and embryonic GnRH neurons (Kusano et al., 1995). Although we made no specific attempts to separate these currents, the delay in K^+ channel activation and the sensitivity of the spike-induced I_K to TEA suggest that the delayed-rectifying I_K is critical for spike repolarization in GT1 neurons. This is consistent with the ability of TEA to facilitate AP-driven Ca^{2+} signals in GT1 neurons (Charles and Hales, 1995). The role of other voltage-gated K^+ channels in the control of spike duration and baseline potential in GT1 neurons requires further investigation.

In addition to voltage-gated K^+ channels, Ca^{2+}-activated K^+ channels participate in the control of AP duration and the associated Ca^{2+} signal. In GT1 neurons, it has been demonstrated that small-conductance, apamin-sensitive K^+ channels (SK channels) contribute to spike repolarization during broad but not sharp AP firing (Van Goor et al., 1999a). In the present study, however, we did not observe a

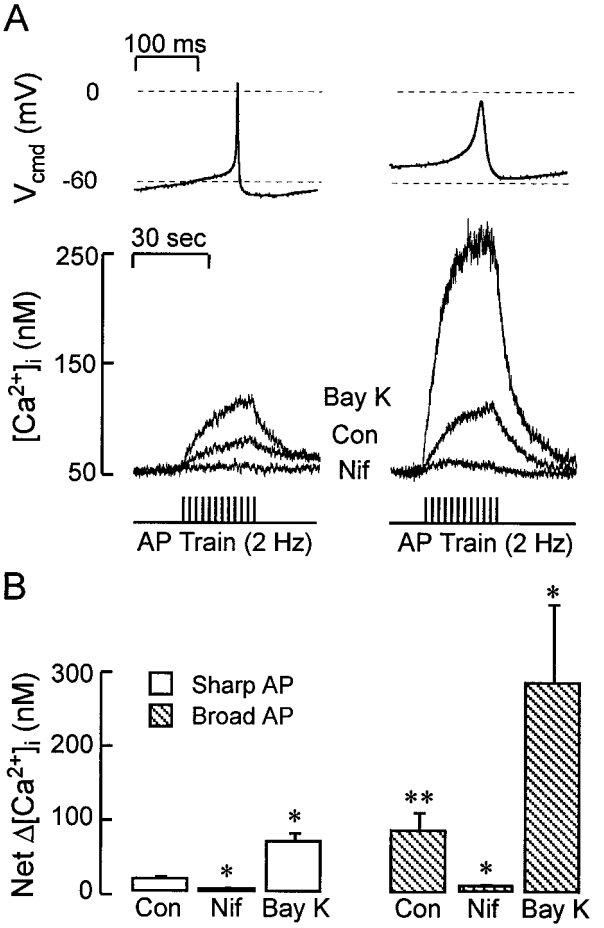

FIGURE 9 Dependence of calcium signaling on the profile of the AP waveform in GT1 neurons. A train of 60 sharp or broad AP waveforms was given at a frequency of 2 Hz under total current recording conditions. (*A*) Representative $[Ca^{2+}]_i$ traces (*bottom*) evoked by the sharp and broad AP train before (Con) and after application of 1 μM nifedipine (Nif) or 1 μM Bay K 8644 (Bay K). All $[Ca^{2+}]_i$ tracings are from the same cell. (*B*) Net change in peak $[Ca^{2+}]_i$ (mean ± SEM, $n = 6$) during the sharp (□) and broad (▨) AP trains before (Con) and after the application of 1 μM nifedipine or Bay K 8644. Double asterisks denote a significant difference between controls in the sharp and broad treatment groups, and single asterisks denote significant difference compared with control values in the same group ($p < 0.01$, paired *t*-test).

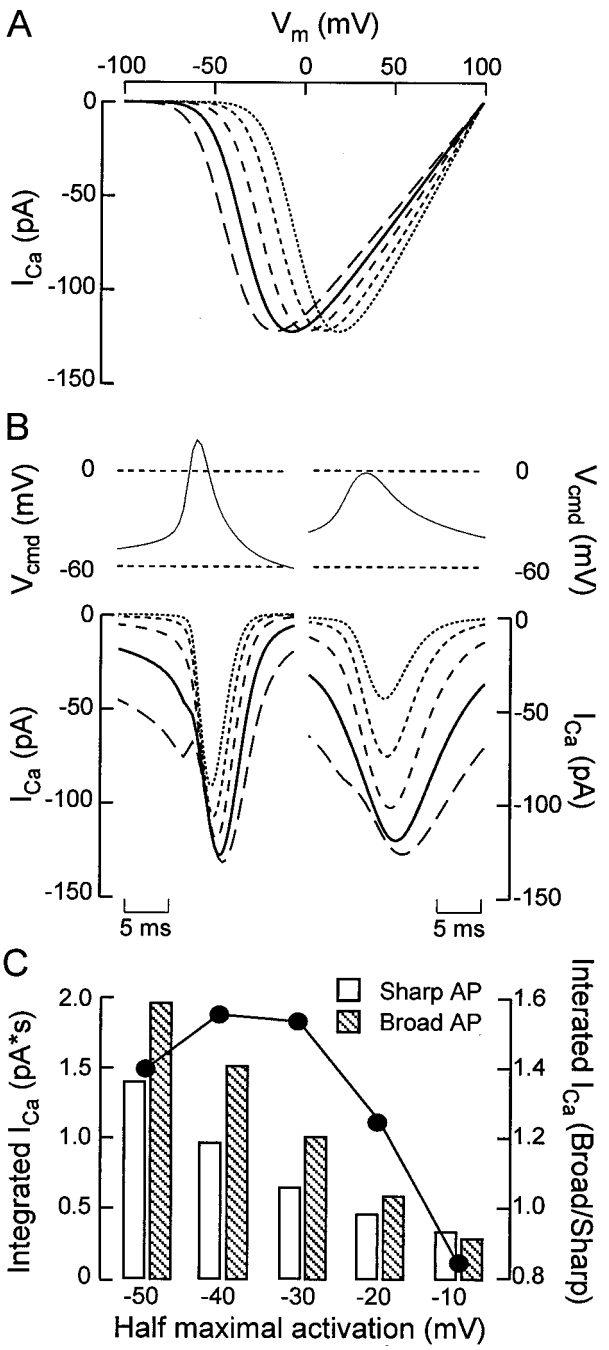

FIGURE 10 Effect of voltage sensitivity of L-type Ca^{2+} current on Ca^{2+} influx. (*A*) Steady-state current-voltage (*I–V*) curves. The solid line is the *I–V* curve for the standard model (half-maximum activation = −40 mV). By shifting the activation properties of the current, we obtained the alternate *I–V* curves (*long, medium, and short dashed, and dotted* = −50, −30, −20, and −10 mV, respectively; see the Appendix for further details). (*B*) Sharp (*left*) and broad (*right*) APs (*upper traces*) were injected into the model with varying L-type Ca^{2+} current-voltage sensitivities. Lower traces show resultant Ca^{2+} currents. Line types correspond to those in *A*. (*C*) Total Ca^{2+}, for sharp (□) and broad (▨) AP trains, from integrating curves in *B*. The curve shows the ratio of integrated Ca^{2+} for broad to sharp spikes. Note that the curve peaks at −40 mV, the standard model value.

significant Ca^{2+}-sensitive outward current during the application of sharp or broad spike trains (data not shown). Similarly, apamin has no effect on the current-voltage relation in GT1 neurons (Spergel et al., 1996). This is most likely due to the requirement for sustained firing of broad APs to elevate $[Ca^{2+}]_i$ to the levels required for activation of the SK channels. During the intermittent application of the AP waveforms used in this study, it is unlikely that such levels would be attained. In addition to SK channels, large-conductance, Ca^{2+}-activated K^+ channels (BK channel) have been identified in GT1 neurons (Spergel et al., 1996), but they do not participate in spontaneous or agonist-induced AP firing (Van Goor et al., 1999a).

In general, the pattern of AP-driven Ca^{2+} signaling in excitable cells is determined by the AP profile and gating properties of the underlying VGCCs. Using the AP clamp technique in combination with the GT1 cell model, we have shown that spike broadening increases the integrated I_{Ca} to facilitate voltage-gated Ca^{2+} entry. Based on the biophysical and pharmacological properties of I_{Ca} in these cells, it has been concluded that only L- and T-type Ca^{2+} channels are expressed in the plasma membrane (Bosma, 1993; Hales et al., 1994; Van Goor et al., 1999b; Costantin and Charles, 1999). The fraction of available T-type Ca^{2+} channels decreases sharply within the range of baseline potentials observed in GT1 neurons, and their participation in AP firing is probably similar to that of I_{Na}. Therefore, in addition to the reduction in peak spike amplitude, the inactivation of T-type Ca^{2+} channels in response to receptor-mediated and non-receptor-mediated V_m depolarization may also partially explain the decrease in peak I_{Ca}. In contrast, the L-type Ca^{2+} channel inactivates very slowly and exhibits little or no steady-state inactivation between the baseline potentials reached during unstimulated or agonist-stimulated AP firing (Van Goor et al., 1999b). Consequently, voltage-gated Ca^{2+} entry during the sharp spike is probably due to activation of both T- and L-type Ca^{2+} channels, whereas the L-type I_{Ca} is the primary current contributing to Ca^{2+} entry during broad spikes.

The influence of AP broadening on the duration and amplitude of the underlying I_{Ca} varies among the different cell types examined. This may be due to differences in the activation properties of the voltage-gated Ca^{2+} channel subtype(s) or isoforms expressed in a particular cell type. For example, several L-type Ca^{2+} channel isoforms have been identified, all of which exhibit different activation and inactivation properties and sensitivities to dihydropyridine agonists and antagonists (Wheeler et al., 1995; Catterall, 1998). In GT1 cells, the activation threshold and peak amplitude of the L-type I_{Ca} is shifted in the hyperpolarizing direction compared to that in other cell types (Van Goor et al., 1999b). In our GT1 cell model, incremental shifts in the half-maximum activation of the L-type Ca^{2+} channels in the depolarizing direction caused a progressive reduction in the ability of AP broadening to enhance voltage-gated Ca^{2+} entry. When the current-voltage relation more closely resembled that of classical L-type Ca^{2+} channels, the sharp AP spike drove more Ca^{2+} entry than the broad waveform. These results suggest that the activation properties of the L-type Ca^{2+} channel isoform expressed in a particular cell type can determine the impact of AP broadening on voltage-gated Ca^{2+} entry.

APPENDIX

The equation for membrane potential (V_m) is

$$C_m \frac{dV_m}{dt} = I_{app} - I_{ionic},$$

where C_m (14 pF) is the membrane capacitance, I_{app} is the applied current, and I_{ionic} is the sum of the ionic currents, given by

$$I_{ionic} = I_{Na} + I_{CaL} + I_{CaT} + I_{KDR} + I_M + I_M + I_{ir} + I_d.$$

I_{Na} is the TTX-sensitive Na^+ current, I_{CaL} and I_{CaT} are the L- and T-type Ca^{2+} currents, respectively, and I_{KDR}, I_M, and I_{ir} are the delayed rectifier, M-type, and inward rectifier K^+ currents, respectively. Finally, I_d is a Ca^{2+}-carrying, inward leak current.

Initially, a conventional Hodgkin-Huxley-like model for I_{Na} (in pA) was used:

$$I_{Na} = g_{Na} m_{Na}^3 h_{Na} (V_m - E_{Na}),$$

where g_{Na} (60 nS) is the conductance, m_{Na} and h_{Na} are the activation and inactivation gating variables, respectively, and E_{Na} (60 mV) is the reversal potential for Na^+. Similar equations govern the other currents (all in pA):

$$I_{CaL} = g_{CaL} m_{CaL}^2 (V_m - E_{Ca}),$$

$$I_{CaT} = g_{CaT} m_{CaT}^2 h_{CaT} (V_m - E_{Ca}),$$

$$I_{KDR} = g_{KDR} n_{KDR}^4 h_{KDR} (V_m - E_K),$$

$$I_M = g_M n_M (V_m - E_K),$$

$$I_{ir} = g_{ir} n_{ir_\infty} (V_m - E_K),$$

$$I_d = g_d (V_m - E_{Ca}),$$

where $g_{CaL} = 1.3$ nS, $E_{Ca} = 100$ mV, $g_{CaT} = 0.94$ nS, $g_{KDR} = 20$ nS, $E_K = -80$ mV, $g_M = 4$ nS, $g_{ir} = 1.71$ nS, and $g_d = 0.044$ nS. The equation for each of the gating variables is

$$\frac{dx}{dt} = \frac{x_\infty - x}{\tau_x},$$

where x represents the activation variables m_{Na}, m_{CaL}, m_{CaT}, n_{KDR}, and n_M, and the inactivation variables h_{Na}, h_{CaT}, and h_{KDR} (when present). Note that for I_{ir} the gating variable is automatically set to its steady-state value.

The steady-state (x_∞) functions are

$$m_{Na_\infty} = (1 + \exp(-(V_m + 42.1)/4.3))^{-1},$$

$$h_{Na_\infty} = (1 + \exp((V_m + 68.2)/10.8))^{-1},$$

$$m_{CaL_\infty} = (1 + \exp(-(V_m - V_h)/12))^{-1}$$

(where V_h is the half-maximum activation of $m_{CaL\infty}$),

$$m_{CaT_\infty} = (1 + \exp(-(V_m + 56.1)/10))^{-1},$$

$$h_{CaT_\infty} = (1 + \exp((V_m + 86.4)/4.7))^{-1},$$

$$n_{KDR_\infty} = (1 + \exp(-(V_m + 25)/15))^{-1},$$

$$h_{KDR_\infty} = 0.7/(1 + \exp(-(V_m + 35)/10))^{-1} + 0.3,$$

$$n_{M_\infty} = (1 + \exp(-(V_m + 37)/4))^{-1},$$

$$n_{ir_\infty} = 0.8(1 + \exp((V_m + 80)/12))^{-} + 0.2.$$

Under normal conditions, V_h in the equation for $m_{CaL\infty}$ was -40 mV. In Fig. 10, V_h was varied between -50 mV and -20 mV to shift the voltage sensitivity of the L-type Ca^{2+} channel in the model GT1 cell.

The functions for the time constants (τ_x, in ms) are

$$\tau_{m_{Na}} = 4.3/(\exp((V_m + 47)/11) + 2\exp(-2(V_m + 47)/11)) + 0.1,$$

$$\tau_{h_{Na}} = 150/(\exp((V_m + 80)/19) + 2\exp(-2(V_m + 80)/19)),$$

$$\tau_{m_{CaL}} = 5/(\exp((V_m + 15)/25) + \exp(-(V_m + 15)/25)),$$

$$\tau_{m_{CaT}} = 7/(\exp((V_m + 50)/9) + \exp(-(V_m + 50)/9)) + 0.8,$$

$$\tau_{h_{CaT}} = 22,$$

$$\tau_{n_{KDR}} = 15/(\exp((V_m + 30)/15) + \exp(-(V_m + 30)/15)) + 1,$$

$$\tau_{h_{KDR}} = 1000,$$

$$\tau_{n_M} = 80/(\exp((V_m + 30)/15) + \exp(-(V_m + 30)/15)).$$

As described in the text, the Hodgkin-Huxley-like Na^+ channel description was unable to fully explain GT1 cell behavior and was replaced with a model adapted from Kuo and Bean (1994). The model proposed by Kuo and Bean, derived from data for rat hippocampal CA1 neurons, displays behavior consistent with that observed in GT1 cells, but there are quantitative differences. We currently lack the data required to fit the mechanistic Kuo and Bean model. Consequently, we developed a phenomenological model that retains the critical elements of nonindependence of I_{Na} activation and inactivation, and in which the channel undergoes a voltage-dependent deactivation transition before recovery from inactivation, as shown in the following reaction scheme:

$$\begin{array}{ccc} D & \underset{\beta(V)}{\overset{\alpha(V)}{\rightleftharpoons}} & A \\ {\scriptstyle k_2^-}\uparrow\downarrow{\scriptstyle k_2} & & {\scriptstyle k_1^-}\uparrow\downarrow{\scriptstyle k_1} \\ D^* & \underset{\beta(V)/a}{\overset{\alpha(V)\cdot a}{\rightleftharpoons}} & A^*, \end{array}$$

where the states are deactivated (D), activated (A), deactivated-inhibited (D*), and activated-inhibited (A*), and the transition rates (in ms) are

$$\alpha = 10/(1 + \exp(-(V_m + 6)/10)),$$

$$\beta = 10/(1 + \exp((V_m + 54.4)/4.6)),$$

$$k_1 = 0.3, \quad k_1^- = 0.03, \quad k_2 = 0.001, \quad \text{and} \quad k_2^- = 0.01,$$

and the correction for microscopic reversibility is

$$a = (k_1 k_2^- / (k_1^- k_2))^{0.5}.$$

D* and A* represent states in which the inactivation particle is bound to the channel and corresponds to the open-inactivated and closed-inactivated states in Kuo and Bean (1994). In fitting the model we found that using three subunits easily gave a good fit to the available experimental data. The revised Na^+ current is given by

$$I_{Na} = g_{Na} O (V_m - E_{Na}),$$

where O is the fraction of conducting channels and is given by A^3 in the reaction scheme.

REFERENCES

Aldrich, R. W., D. P. Corey, and C. F. Stevens. 1983. A reinterpretation of mammalian sodium channel gating based on single channel recording. *Nature.* 306:436–441.

Augustine, G. J. 1990. Regulation of transmitter release at the squid giant synapse by presynaptic delayed rectifier potassium current. *J. Physiol. (Lond.).* 431:343–364.

Barry, P. H. 1994. JPCalc, a software package for calculating liquid junction potential corrections in patch-clamp, intracellular, epithelia and bilayer measurements. *J. Neurosci. Methods.* 51:107–116.

Bezanilla, F., and C. M. Armstrong. 1977. Inactivation of the sodium channel. I. Sodium current experiments. *J. Gen. Physiol.* 70:549–566.

Bosma, M. M. 1993. Ion channel properties and episodic activity in isolated immortalized gonadotropin-releasing hormone (GnRH) neurons. *J. Membr. Biol.* 136:85–96.

Callaway, J. C., and W. N. Ross. 1995. Frequency dependent propagation of sodium action potentials in dendrites of hippocampal CA1 pyramidal neurons. *J. Neurophysiol.* 74:1395–1403.

Cantrell, A. R., T. Scheuer, and W. A. Catterall. 1999. Voltage-dependent neuromodulation of Na^+ channels by D1-like dopamine receptors in rat hippocampal neurons. *J. Neurosci.* 19:5301–5310.

Catterall, W. A. 1998. Structure and function of neuronal Ca^{2+} channels and their role in neurotransmitter release. *Cell Calcium.* 24:307–323.

Charles, A., and T. G. Hales. 1995. Mechanisms of spontaneous calcium oscillations and action potentials in immortalized hypothalamic (GT1–7) neurons. *J. Neurophysiol.* 73:56–64.

Charles, A. C., E. T. Piros, C. J. Evans, and T. G. Hales. 1999. L-type Ca^{2+} channels and K^+ channels specifically modulate the frequency and amplitude of spontaneous Ca^{2+} oscillations and have distinct roles in prolactin release in GH_3 cells. *J. Biol. Chem.* 274:7508–7515.

Colbert, C. M., J. C. Magee, D. A. Hoffman, and D. Johnston. 1997. Slow recovery from inactivation of Na^+ channels underlies the activity-dependent attenuation of dendritic action potentials in hippocampal CA1 pyramidal neurons. *J. Neurosci.* 17:6512–6521.

Costantin, J. L., and A. C. Charles. 1999. Spontaneous action potentials initiate rhythmic intercellular calcium waves in immortalized hypothalamic (GT1–1) neurons. *J. Neurophysiol.* 82:429–435.

De Konninck, P., and H. Schulman. 1998. Sensitivity of CAM kinase II to the frequency of Ca^{2+} oscillations. *Science.* 279:227–230.

Dolmetsch, R. E., R. S. Lewis, C. C. Goodnow, and J. I. Healy. 1997. Differential activation of transcription factors induced by Ca^{2+} response amplitude and duration. *Nature.* 386:855–858.

Gao, B.-X., and L. Ziskind-Conhaim. 1998. Development of ionic current underlying changes in action potential waveforms in rat spinal motoneurons. *J. Neurophysiol.* 80:3047–3061.

Goldsmith, B. A., and T. W. Abrams. 1992. cAMP modulates K^+ currents, increasing spike duration and excitability in *Aplysia* sensory neurons. *Proc. Natl. Acad. Sci. USA.* 89:11481–11485.

Hales, T. G., M. J. Sanderson, and A. C. Charles. 1994. GABA has excitatory actions on GnRH-secreting immortalized hypothalamic (GT1–7) neurons. *Neuroendocrinology.* 59:297–308.

Hodgkin, A. L., and A. F. Huxley. 1952. A quantitative description of membrane current and its application to conduction and excitation in nerve. *J. Physiol. (Lond.).* 117:500–544.

Hsu, S.-F., G. J. Augustine, and M. B. Jackson. 1996. Adaptation of Ca^{2+}-triggered exocytosis in presynaptic terminals. *Neuron.* 17: 501–512.

Irisawa, H., H. F. Brown, and W. Giles. 1993. Cardiac pacemaking in the sinoatrial node. *Physiol. Rev.* 73:197–227.

Jackson, M. B., A. Konnerth, and G. J. Augustine. 1991. Action potential broadening and frequency-dependent facilitation of calcium signals in pituitary nerve terminals. *Proc. Natl. Acad. Sci. USA.* 88:380–384.

Johnston, D., D. A. Hoffman, C. M. Colbert, and J. C. Magee. 1999. Regulation of back-propagating action potentials in hippocampal neurons. *Curr. Opin. Neurobiol.* 9:288–292.

Jung, H.-Y., T. Mickus, and N. Sprustson. 1997. Prolonged sodium channel inactivation contributes to dendritic action potential attenuation in hippocampal pyramidal neurons. *J. Neurosci.* 17:6639–6646.

Kao, J. P. Y. 1994. Practical aspects of measuring $[Ca^{2+}]_i$ with fluorescent indicators. *Methods Cell Biol.* 40:155–181.

Kuo, C.-C., and B. P. Bean. 1994. Na^+ channels must deactivate to recover from inactivation. *Neuron.* 12:819–829.

Kuryshev, Y., L. Haak, G. V. Childs, and A. K. Ritchie. 1997. Corticotropin releasing hormone inhibits inwardly rectifying potassium current in rat corticotropes. *J. Physiol. (Lond.).* 502.2:265–279.

Kusano, K., S. Fueshko, H. Gainer, and S. Wray. 1995. Electrical and synaptic properties of embryonic luteinizing hormone-releasing hormone neurons in explant cultures. *Proc. Natl. Acad. Sci. USA.* 92: 3912–3918.

Magee, J., D. Hoffman, C. Colbert, and D. Johnston. 1998. Electrical and calcium signaling in dendrites of hippocampal pyramidal neurons. *Annu. Rev. Physiol.* 60:327–346.

McCobb, D. P., and K. G. Beam. 1991. Action potential waveform voltage-clamp commands reveal striking differences in calcium entry via low and high voltage-activated calcium channels. *Neuron.* 7:119–127.

Mellon, P. L., J. J. Windle, P. C. Goldsmith, C. A. Padula, J. L. Roberts, and R. I. Weiner. 1990. Immortalization of hypothalamic GnRH neurons by genetically targeted tumorigenesis. *Neuron.* 5:1–10.

Nathan, R. D. 1986. Two electrophysiologically distinct type of cultured pacemaker cells from rabbit sinoatrial node. *Am. J. Physiol.* 250: H325–H329.

Park, D., and K. Dunlap. 1998. Dynamic regulation of calcium influx by G-proteins, action potential waveform, and neuronal firing frequency. *J. Neurosci.* 18:6757–6766.

Poolos, N. P., and D. Johnston. 1999. Calcium-activated potassium conductances contribute to action potential repolarization at the soma but not the dendrites of hippocampal CA1 pyramidal neurons. *J. Neurosci.* 19:5205–5212.

Rae, J., K. Cooper, P. Gates, and M. Watsky. 1991. Low access resistance perforated patch recording using amphotericin B. *J. Neurosci. Methods.* 37:15–26.

Raman, I. M., and B. P. Bean. 1997. Resurgent sodium current and action potential formation in dissociated cerebellar Purkinje neurons. *J. Neurosci.* 17:4517–4526.

Raman, I. M., and B. P. Bean. 1999. Ionic currents underlying spontaneous action potentials in isolated cerebellar purkinje neurons. *J. Neurosci.* 19:1663–1674.

Sankaranarayanan, S., and S. M. Simasko. 1996. Characterization of an M-like current modulated by thyrotropin-releasing hormone in normal rat lactotrophs. *J. Neurosci.* 16:1668–1678.

Spencer, A. N., J. Przysiezniak, J. Acosta-Urquike, and T. A. Basarsky. 1989. Presynaptic spike broadening reduces junctional potential amplitude. *Nature.* 340:636–638.

Spergel, D. J., K. J. Catt, and E. Rojas. 1996. Immortalized GnRH neurons express large-conductance calcium-activated potassium channels. *Neuroendocrinology.* 63:101–111.

Spruston, N., Y. Schiller, G. Stuart, and B. Sakmann. 1995. Activity-dependent action potential invasion and calcium influx into hippocampal CA1 dendrites. *Science.* 268:297–300.

Toth, P. T., and R. J. Miller. 1995. Calcium and sodium currents evoked by action potential waveforms in rat sympathetic neurons. *J. Physiol. (Lond.).* 485.1:43–57.

Van Goor, F., L. Z. Krsmanovic, K. J. Catt, and S. S. Stojilkovic. 1999a. Coordinate regulation of gonadotropin-releasing hormone neuronal firing patterns by cytosolic calcium and store depletion. *Proc. Natl. Acad. Sci. USA.* 96:4101–4106.

Van Goor, F., L. Z. Krsmanovic, K. J. Catt, and S. S. Stojilkovic. 1999b. Control of action potential-driven calcium influx in GT1 neurons by the activation status of sodium and calcium channels. *Mol. Endocrinol.* 13:587–603.

Westenbroek, R. E., D. K. Merrick, and W. A. Catterall. 1989. Differential subcellular localization of R_I and R_{II} Na^+ channel subtypes in central neurons. *Neuron.* 3:695–704.

Wheeler, D. B., A. Randall, W. A. Sather, and R. W. Tsien. 1995. Neuronal calcium channels encoded by the α_{1A} subunit and their contribution to excitatory synaptic transmission in the CNS. *Prog. Brain Res.* 105: 65–78.